Tunable Two-Way Unidirectional Acoustic Diodes: Design and Simulation

Article *in* Journal of Applied Mechanics · December 2018

DOI: 10.1115/1.4042321

CITATIONS
16

READS
397

4 authors:

Yingjie Chen
Zhejiang University
8 PUBLICATIONS **29** CITATIONS
SEE PROFILE

Bin Wu
National University of Ireland, Galway
45 PUBLICATIONS **334** CITATIONS
SEE PROFILE

Yipin Su
National University of Ireland, Galway
27 PUBLICATIONS **232** CITATIONS
SEE PROFILE

W. Q. Chen
Zhejiang University
587 PUBLICATIONS **11,294** CITATIONS
SEE PROFILE

Yingjie Chen
Key Laboratory of Soft Machines and Smart Devices of Zhejiang Province, Zhejiang University, Hangzhou, 310027, China;
Department of Engineering Mechanics, Zhejiang University, Hangzhou, 310027, China

Bin Wu
Department of Mechanical and Aerospace Engineering, Politecnico di Torino, Torino, 10129, Italy

Yipin Su
Key Laboratory of Soft Machines and Smart Devices of Zhejiang Province, Zhejiang University, Hangzhou, 310027, China;
Department of Engineering Mechanics, Zhejiang University, Hangzhou, 310027, China;
School of Mathematics, Statistics and Applied Mathematics, NUI Galway, University Road, Galway, H91 TK33, Ireland

Weiqiu Chen[1]
Key Laboratory of Soft Machines and Smart Devices of Zhejiang Province, Zhejiang University, Hangzhou, 310027, China;
State Key Lab of CAD and CG, Zhejiang University, Hangzhou, 310058, China;
Department of Engineering Mechanics, Zhejiang University, Hangzhou, 310027, China;
Soft Matter Research Center, Zhejiang University, Hangzhou, 310027, China
e-mail: chenwq@zju.edu.cn

Tunable Two-Way Unidirectional Acoustic Diodes: Design and Simulation

Predeformation simultaneously changes the effective material stiffness as well as the geometric configuration and therefore may be utilized to tune wave propagation in soft phononic crystals (PCs). Moreover, the band gaps of soft PCs, as compared with those of the hard ones, are more sensitive to the external mechanical stimuli. A one-dimensional tunable soft acoustic diode based on soft functionally graded (FG) PCs is proposed. The two-way asymmetric propagation behavior is studied at the resonant frequency within the band gap. Numerical results show that the operating frequency (i.e., the resonant peak) of the soft graded acoustic diode can be altered by adjusting the mechanical biasing fields (including the longitudinal prestress and the lateral equibiaxial tension). The adjustment becomes significant when the strain-stiffening effect of the Gent hyperelastic material is properly harnessed. Furthermore, the prestress or equibiaxial tension can affect the two-way filtering of the soft FG PC in a separate and different manner. In addition, it is much easier to realize the tunable acoustic diode by exploiting soft FG materials with stronger compressibility. It is shown that the introduction of acoustic impedance is beneficial for predicting the tunable effects. The simulations and conclusions should provide a solid guidance for the design of tunable two-way unidirectional acoustic diodes made from soft hyperelastic materials. [DOI: 10.1115/1.4042321]

Keywords: tunable acoustic diode, functionally graded, phononic crystal, soft material, biasing field

1 Introduction

Phononic crystals (PCs) have attracted considerable attention from academia and industry alike due to their unique acoustic properties since first proposed by Kushwaha et al. [1] in the 1990s. Based on the Bragg scattering mechanism or the locally resonant mechanism [2], acoustic/elastic waves are prohibited to propagate within certain frequency ranges, which are called band gaps in PCs. This phenomenon can be used to design functional devices such as acoustic diodes [3,4], acoustic cloaks [5–7], and directional radiation devices [8,9].

Functionally graded materials (FGMs) are one particular type of advanced engineering materials exhibiting inhomogeneous material properties, which vary continuously in one or more directions. FGMs were first proposed and prepared by a group of Japanese material scientists in the middle of 1980s, and since then they have been widely used in aerospace, aircraft, civil engineering, and chemical industry [10–12]. Compared with the traditional materials, FGMs can be designed to reduce thermal stresses, eliminate the sharp stress discontinuity, and increase the bonding strength. Due to their excellent properties, many works have been carried out to investigate elastic wave propagation in FGM structures. Chen et al. [13] presented a hybrid strategy by combining the reverberation-ray matrix method and the state-space method so as to obtain stable numerical results for waves propagating in an elastic FGM plate at both small and large frequencies. Cao et al. [14] studied Lamb wave propagation in a functionally graded (FG) piezoelectric–piezomagnetic plate and presented the influences of the gradient parameter on the dispersion curves. In recent years, some efforts have been devoted to the study of wave propagation in FG PCs. Fomenko et al. [15] considered the effects of geometric and material parameters on the transmission behaviors and band structures of the in-plane elastic waves in FG PCs. Guo et al. [16] discussed the impacts of FG interlayers on the dispersion relations of elastic waves in one-dimensional

[1]Corresponding author.

Contributed by the Applied Mechanics Division of ASME for publication in the Journal of Applied Mechanics. Manuscript received November 12, 2018; final manuscript received December 16, 2018; published online January 8, 2019. Editor: Yonggang Huang.

piezoelectric/piezomagnetic PCs. Based on a graded PC plate, Torrent et al. [17] designed an omnidirectional refractive device for flexural waves in a thin plate. Liang et al. [18] constructed an acoustic absorber by means of spatially varying refractive index.

Similar to the electrical and photonic devices, acoustic or mechanical diodes can allow the acoustic or elastic waves to propagate unidirectionally only in a certain frequency range. Many works have been conducted to study the wave propagation characteristics in acoustic or mechanical diodes made of nonlinear media. Liang et al. [19] presented an acoustic diode which couples a superlattice with a nonlinear medium and investigated the transmission of acoustic waves as a function of frequency. Li et al. [20] constructed a sonic-crystal-based acoustic diode which breaks the spatial inversion symmetry and realized experimentally the sound unidirectional transmission. Li et al. [21] recently studied the nonreciprocal wave phenomenon in a nonlinear acoustic metamaterial which is composed of a linear PC and a nonlinear layer.

In our previous work [22], we proposed a two-way acoustic filter for unidirectional transmission at the resonant frequency peak within a band gap of the FG PC. The mechanism is that the spatial symmetry of the PC is broken owing to the introduction of FG properties. We found that the left-moving wave at a resonant frequency peak is able to pass through the finite structure via resonance, while the right-moving wave at the same frequency will be blocked due to Bragg scattering, and vice versa. If we replace the FGM with a homogeneous material, the transmission spectra for waves propagating in opposite directions will be identical, and as a result, there will be no unidirectional transmission for waves within the band gap. It is worth noting that the PC in that work is fabricated with traditional linear elastic materials of fixed material and geometrical parameters, thus it is not easy to tune the operating frequency of such an acoustic diode.

In practical industrial applications, the frequencies of acoustic waves in PCs to be filtered are generally complicated and varying in a wide range. In order to realize tunable band gaps, a lot of efforts have been done to design active PCs to satisfy the specific needs, resulting in a revolution of tunable, active, or even smart manipulation of acoustic/elastic waves. Goffaux and Vigneron [23] proposed the concept of tunable PCs for the first time and realized the tunability of band structures by rotating the solid square scatters in an air/solid PC. Taking the magneto-electro-elastic couplings into account, Wang et al. [24] investigated the elastic wave propagation in PCs with piezoelectric and piezomagnetic inclusions.

The band gaps in soft PCs are more sensitive to external stimuli (e.g., mechanical loadings, electric biasing fields, light signals, and temperature) than those in PCs made of hard materials. Recently, soft PCs are attracting more and more interests from scientists and engineers [25–27]. For the purpose of broadening the tunable range of band gaps, it is of great importance to pay attention to actively tunable PCs made of soft materials. Based on the finite deformation theory formulated by Ogden [28], Huang et al. [29] showed that the band gaps of one-dimensional hyperelastic PCs can be effectively tuned by adjusting the magnitude of the longitudinal prestress while fixing the lateral equibiaxial deformation. Galich et al. [30] further analyzed the tunable band gaps in soft PCs of hyperelastic materials with different constitutive models and concluded that the finite predeformation simultaneously changes the effective material properties and filling ratio of PCs, and as a result tunes the band gaps. Wu et al. [31] employed the nonlinear electroelasticity theory and its incremental theory [32,33] to investigate the propagation of longitudinal waves in a soft electroactive PC cylinder subject to a combination of axial force and electric field. Zhu et al. [34] explored the tuning effect of the biasing electric displacement on obliquely incident SH waves propagating in periodic dielectric elastomer laminates. Bian et al. [35] investigated the thermally tunable band gaps in one-dimensional PCs composed of two alternating heat sensitive phases. It is worth mentioning that Wu et al. [36] recently analyzed the axisymmetric guided waves in a pressurized FG elastomeric hollow cylinder and presented a fascinating conclusion that material tailoring can be utilized to manipulate elastic wave propagations along with the adjustment of prestretch and pressure difference.

In this paper, we propose a compressible FG hyperelastic PC to study how mechanical biasing fields can be utilized to tune the propagation of longitudinal waves and obtain a tunable two-way acoustic filter or diode with a wide range of working frequency. It should be pointed out that, to focus on longitudinal waves, we have to consider compressible materials in the PC to ensure the existence of pressure waves [30]. Nonlinear elasticity theory and its incremental version are adopted to capture the material and geometric nonlinearities of the soft PCs. The mechanism of the active control of band gaps is easily understandable: the application of mechanical loadings changes the geometry (filling ratio) and effective material properties of the soft PCs, which in turn affects the band gaps. We find that the propagation of longitudinal waves in soft PCs can be significantly affected by the combination of the mechanical biasing fields and the material gradient characteristics.

This paper is structured as follows: Section 2 describes the basic formulations of nonlinear elasticity theory and the associated linearized incremental theory. In the same section, we also obtain the band structure of a nongraded periodic structure and the transmission relation of a finite graded structure by using the state-space method. Numerical results are presented in Sec. 3 to elucidate the effects of the mechanical biasing fields as well as the Poisson's ratio on the wave transmission behavior in soft FG PCs. Finally, in Sec. 4, we draw some conclusions.

2 Theoretical Model and Analysis

2.1 Brief Introduction to Nonlinear Elasticity and Incremental Wave Motion. Consider a soft continuum body, with each point in the undeformed or reference configuration labeled by its position vector $\mathbf{X}$. As the body undergoes deformation, the particle at $\mathbf{X}$ in the reference configuration moves to a new position $\mathbf{x}$ in the current configuration, by the following mapping:

$$\mathbf{x} = \boldsymbol{\chi}(\mathbf{X}, t) \tag{1}$$

In the absence of body force, the equilibrium equation reads

$$\mathrm{Div}\mathbf{T} = \mathbf{0} \tag{2}$$

where Div denotes the divergence operator with respect to the reference configuration. The nominal stress tensor $\mathbf{T}$ and the Cauchy stress tensor $\boldsymbol{\tau}$ are connected by

$$\mathbf{T} = J\mathbf{F}^{-1}\boldsymbol{\tau} \tag{3}$$

where $\mathbf{F} = \partial\mathbf{x}/\partial\mathbf{X}$ is the deformation gradient tensor, with the Jacobian (i.e., local volume change) $J = \det\mathbf{F} > 0$ being its determinant.

The nonlinear constitutive relation for a compressible hyperelastic elastomer is

$$\mathbf{T} = \frac{\partial\Omega}{\partial\mathbf{F}} \tag{4}$$

where Ω is the energy density function. Here, we consider the so-called ideal compressible Gent model [30,37]

$$\Omega = -\frac{\mu}{2}J_m \ln\left(1 - \frac{I_1 - 3}{J_m}\right) - \mu \ln J + \left(\frac{\Lambda}{2} - \frac{\mu}{J_m}\right)(J-1)^2 \tag{5}$$

where μ and Λ are the shear modulus and the first Lamé's parameter of the solid in the undeformed configuration, respectively, and

$I_1 = \lambda_1^2 + \lambda_2^2 + \lambda_3^2$ represents the first invariant. The first Lamé's parameter, Poisson's ratio υ, and shear modulus of the solid are connected via $\Lambda = 2\mu\upsilon/(1-2\upsilon)$. J_m, usually known as the Gent constant, is the dimensionless stiffening parameter of the material. When $J_m \to \infty$, the neo-Hookean model is recovered from Eq. (5). In this paper, we shall utilize the strain-stiffening effect of the Gent materials to obtain a more pronounced tunable effect than other materials (e.g., the neo-Hookean materials) through the adjustment of the mechanical biasing fields.

By using Eqs. (3)–(5), the principal Cauchy stress components can be obtained as [31]

$$\begin{aligned}
\tau_{11} &= \frac{\mu J_m}{J_m - I_1 + 3} J^{-1}\lambda_1^2 - \mu J^{-1} + \left(\Lambda - \frac{2\mu}{J_m}\right)(J-1) \\
\tau_{22} &= \frac{\mu J_m}{J_m - I_1 + 3} J^{-1}\lambda_2^2 - \mu J^{-1} + \left(\Lambda - \frac{2\mu}{J_m}\right)(J-1) \\
\tau_{33} &= \frac{\mu J_m}{J_m - I_1 + 3} J^{-1}\lambda_3^2 - \mu J^{-1} + \left(\Lambda - \frac{2\mu}{J_m}\right)(J-1)
\end{aligned} \tag{6}$$

Consider an infinitesimal incremental perturbation $\dot{\mathbf{x}}$ superimposed on the finite predeformation. The linear governing equation of any incremental wave motion is

$$\mathrm{Div}\dot{\mathbf{T}} = \rho_0 \dot{\mathbf{x}}_{,tt} \tag{7}$$

where the superposed dot indicates an incremental physical quantity, the subscript comma indicates differentiation with respect to the variables that follow, and ρ_0 denotes the mass density of the solid in the reference configuration. The expression for the incremental nominal stress is

$$\dot{\mathbf{T}} = \mathbf{A}\dot{\mathbf{F}} \tag{8}$$

where $\dot{\mathbf{F}} = \mathrm{Grad}\mathbf{u}$ is the incremental deformation gradient tensor, with $\mathbf{u}(\mathbf{x},t) = \dot{\mathbf{x}}(\mathbf{X},t)$ being the incremental displacement, and $\mathbf{A}$ is a fourth-order referential elastic tensor, with components as follows:

$$A_{aibj} = \frac{\partial^2 \Omega}{\partial F_{ia} \partial F_{jb}} \tag{9}$$

The Eulerian counterpart of Eq. (7) is

$$\mathrm{div}\dot{\mathbf{T}}_0 = \rho \mathbf{u}_{,tt} \tag{10}$$

where $\dot{\mathbf{T}}_0 = \mathbf{A}_0 \mathrm{grad}\mathbf{u}$ is the push forward of Eq. (8), div and grad represent the divergence and gradient operators with respect to the current configuration, and $\rho = J^{-1}\rho_0$ is the mass density of the solid in the current configuration. $\mathbf{A}_0$ is the fourth-order instantaneous elastic tensor and is given in component notation by

$$A_{0piqj} = J^{-1} F_{pa} F_{qb} A_{aibj} \tag{11}$$

In summary, the incremental motions of the solid with an underlying large predeformation can be described by the aforementioned formulations (Eqs. (7)–(11)).

2.2 Analysis of Soft Phononic Crystals. As shown in Fig. 1, a PC composed of two alternating compressible hyperelastic materials is investigated. The two material phases are arranged periodically along the x_3 direction and indicated by A and B, respectively. Hereafter, $(\bullet)_p$ (p = A, B) signifies the physical quantities of the p-phase in the PC. Geometrically, the initial lengths of phases A and B are $h_A = \nu_A h$ and $h_B = \nu_B h$, respectively, where h is the initial length of the cell, and ν_A and $\nu_B = 1 - \nu_A$ are the initial volume fractions of phases A and B, respectively. After applying a lateral equibiaxial prestretch λ_1

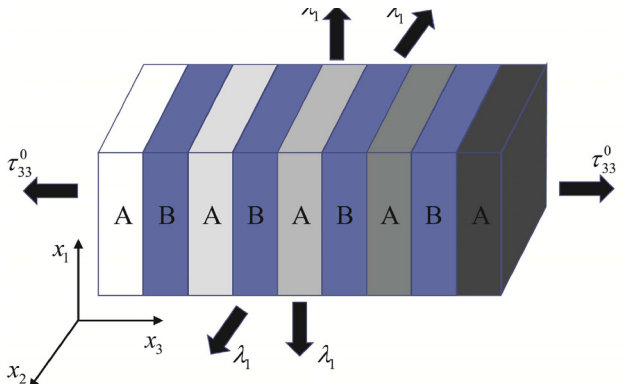

Fig. 1 Diagram of a soft-graded PC under mechanical biasing fields

perpendicular to the x_3 direction and keeping it fixed, the longitudinal waves propagating in the PC can be tuned via the longitudinal mechanical loading τ_{33}^0 along the x_3 direction. According to the expressions for the Cauchy stress components in Eq. (6), we can determine the stretch ratios of the two phases λ_{3A} and λ_{3B} along the x_3 direction once the prestress τ_{33}^0 is given. The deformed thicknesses of phases A and B then become

$$d_A = \lambda_{3A} h_A, \quad d_B = \lambda_{3B} h_B \tag{12}$$

The length of the deformed cell is $d = d_A + d_B$. The deformation gradient tensor of the p-phase can be written as $\mathbf{F}_p = \mathrm{diag}[\lambda_1, \lambda_1, \lambda_{3p}]$. The layers are assumed to be perfectly bonded together. Consequently, we can obtain the associated first invariant and local volume change of the p-phase as follows:

$$I_{1p} = \lambda_1^2 + \lambda_2^2 + \lambda_{3p}^2, \quad J_p = \lambda_1 \lambda_2 \lambda_{3p} \tag{13}$$

For 1D infinite layered PCs made of isotropic hyperelastic materials, if all physical quantities are assumed to be functions of x_3 only, it is easy to know that the longitudinal displacement u_3 is decoupled from the other two displacement components [29,30]. In fact, from Eq. (10) with $\dot{\mathbf{T}}_0 = \mathbf{A}_0 \mathrm{grad}\mathbf{u}$, we can deduce the governing equation for the incremental longitudinal waves propagating along the x_3 direction as

$$A_{03333p} \frac{\partial^2 u_{3p}}{\partial x_3^2} = \rho_p \frac{\partial^2 u_{3p}}{\partial t^2} \tag{14}$$

where the component of the instantaneous elastic tensor A_{03333p} can be written in terms of the principal stretches as

$$\begin{aligned}
A_{03333p} = J_p^{-1} \Bigg[&\frac{\mu_p J_{mp}}{J_{mp} - I_{1p} + 3} \lambda_{3p}^2 + \frac{2\mu_p J_{mp} \lambda_{3p}^4}{(J_{mp} - I_{1p} + 3)^2} + \mu_p \\
&+ \left(\Lambda_p - \frac{2\mu_p}{J_{mp}}\right) J_p^2 \Bigg]
\end{aligned} \tag{15}$$

The state-space method is now adopted to investigate the band structures of infinite nongraded periodic structures and the transmission spectra of finite quasi-periodic FG soft PCs. Assume the x_3 direction to be parallel (or antiparallel) to the direction of wave propagation. The incremental state vector can be defined by

$$\mathbf{V}_t = \begin{Bmatrix} u_{3p} \\ \dot{T}_{033p} \end{Bmatrix} \tag{16}$$

where u_{3p} and $\dot{T}_{033p} = A_{03333p}(\partial u_{3p}/\partial x_3)$ are the incremental displacement and Cauchy stress along the x_3 direction, respectively.

The constitutive relation and the equation of motion can be rewritten as

$$\frac{\partial u_{3p}}{\partial x_3} = \frac{1}{A_{03333p}} \dot{T}_{033p} \tag{17}$$

$$\frac{\partial \dot{T}_{033p}}{\partial x_3} = \rho_p \frac{\partial^2 u_{3p}}{\partial t^2} \tag{18}$$

The time–harmonic displacement of the incremental longitudinal wave can be supposed as

$$u_{3p}(x_3, t) = U_{3p}(x_3)\exp(-i\omega t) \tag{19}$$

Substituting Eq. (19) into Eqs. (17) and (18) as well as eliminating the time factor, we obtain

$$\frac{d}{dx_3}\mathbf{V} = \mathbf{M}\mathbf{V} = \begin{bmatrix} 0 & \dfrac{1}{A_{03333p}} \\ -\rho_p \omega^2 & 0 \end{bmatrix} \mathbf{V} \tag{20}$$

where $\mathbf{M}$ is the coefficient matrix of the p-phase, and $\mathbf{V}$ is the amplitude of $\mathbf{V}_t$.

For the finite FG PCs, it is difficult to achieve the analytical solution directly due to the nonhomogeneous materials involved, for which A_{03333p} is a function of x_3. In this case, the matrix $\mathbf{M}$ is not constant, and the approximate laminate or multilayer technique [38] can be employed to obtain the results close to the original solution. For this purpose, each layer (phase A or B) in the undeformed configuration is equally divided into a few sufficiently thin sublayers. In each sublayer, the material parameters and prestretches are taken to be constants rather than variables, and hence we can determine the deformed length Δd_i of the ith sublayer. Then $\mathbf{M}$ is treated as a constant matrix in each sublayer, and the relation between the state vectors at the two sides of the ith sublayer is established as

$$\mathbf{V}_{(i+1)} = \exp(\mathbf{M}_{im}\Delta d_i)\mathbf{V}_i \tag{21}$$

where $\exp(\mathbf{M}_{im}\Delta d_i)$ denotes the transfer matrix of the ith sublayer, and $\mathbf{M}_{im}$ indicates the constant coefficient matrix within the sublayer which is obtained by letting each variable take its value at the middle point of that sublayer. Finally, utilizing the continuity conditions at each fictitious interface between two sublayers, and those at the interface between phases A and B, we obtain the transfer relationship between the incident side and the exit end as

$$\mathbf{V}_{n+1} = \mathbf{M}_t \mathbf{V}_1 \tag{22}$$

where $\mathbf{M}_t = \Pi_{i=n}^{1} \exp(\mathbf{M}_{im}\Delta d_i)$ is the global transfer matrix and n is the total number of sublayers of the finite structure. It can be seen that $\mathbf{M}_t$ becomes different when the incremental wave propagates in the FG PCs along an opposite direction.

When calculating the band structure of the infinite nongraded PCs, it is enough to consider one unit cell (one layer A and one layer B, both being homogeneous). By exploring the Bloch conditions along with the transfer relation at the two ends of the cell, we can obtain

$$[\mathbf{M}_t - \exp(ikd)\mathbf{I}]\mathbf{V}_L = \mathbf{0} \tag{23}$$

where k is Bloch wave number, $\mathbf{V}_L$ denotes the state vector at the left side of the unit cell, and $\mathbf{I}$ is an identity matrix of dimension 2×2. Here $\mathbf{M}_t$ is the transfer matrix of the unit cell. The existence of nontrivial solutions requires the determinant of the coefficient matrix in Eq. (23) to be zero, i.e.,

$$\det[\mathbf{M}_t - \exp(ikd)\mathbf{I}] = 0 \tag{24}$$

Then, the dispersion relation between k and ω can be achieved by solving the above equation.

To calculate the transmission spectrum of the finite FG PC, we need to prescribe the boundary conditions at the two ends of the structure in addition to the transfer matrix. Here, the incident side is set to have a prescribed incremental displacement, and the exit side is free of stress. Then, the transfer relation between the state vectors at the two ends becomes

$$\begin{Bmatrix} U_3^{(n+1)} \\ 0 \end{Bmatrix} = \begin{bmatrix} M_{t11} & M_{t12} \\ M_{t21} & M_{t22} \end{bmatrix} \begin{Bmatrix} 1 \\ \dot{T}_{033}^{(1)} \end{Bmatrix} \tag{25}$$

where we have assumed the prescribed incremental displacement to be 1 at the incident side, $U_3^{(n+1)}$ and $\dot{T}_{033}^{(1)}$ indicate the incremental displacement at the exit or output side and the incremental Cauchy stress at the incident side, respectively, and M_{tij} are the elements of $\mathbf{M}_t$. Once the geometric size and the mechanical biasing fields of the soft PC are determined, the global transfer matrix and hence the output displacement can be obtained uniquely

$$\begin{aligned} \dot{T}_{033}^{(1)} &= -\frac{M_{t21}}{M_{t22}} \\ U_3^{(n+1)} &= M_{t11} + M_{t12}\dot{T}_{033}^{(1)} \end{aligned} \tag{26}$$

At last, the transmission coefficient is defined by the logarithm of the absolute value of the output incremental displacement over the unit incident displacement

$$P = \ln|U_3^{(n+1)}| = \ln|M_{t11} - M_{t12}M_{t21}/M_{t22}| \tag{27}$$

3 Numerical Results and Discussion

Before discussing the numerical results, we will introduce the following normalized physical quantities indicated by the tilde on the top of the quantities: the dimensionless initial stress $\tilde{\tau}_{33}^0 = \tau_{33}^0/\mu_r$, the density ratio $\tilde{\rho}_0 = \rho_0/\rho_r$, the initial shear modulus ratio $\tilde{\mu} = \mu/\mu_r$, and the normalized frequency and wave number $\tilde{\omega} = \omega h/\sqrt{\rho_r/\mu_r}$ and $\tilde{k} = kh$. Here, we choose the hyperelastic material—the silicon rubber Zhermack Elite Double 32 [30] (with density $\rho_r = 1050$ kg/m^3 and shear modulus $\mu_r = 0.444$ MPa)—as the referential material.

Now, the band structure and the transmission characteristic of wave propagation in the compressible hyperelastic PCs can be studied based on the formulations outlined in Sec. 2. For the nongraded hypothetical materials A and B, the dimensionless densities are taken to be $\tilde{\rho}_{0A} = \tilde{\rho}_{0B} = 1$, and shear moduli are $\tilde{\mu}_A = 2$, $\tilde{\mu}_B = 1$. Moreover, assume $h_A = h_B = 0.5$, $\upsilon_A = \upsilon_B = 1/3$, and $J_{mA} = J_{mB} = 10$. When the dimensionless Gent constant is infinitely large (J_m can be considered as infinite when taking the value of 1000 in the calculations), the Gent model can be reduced to the neo-Hookean model. In this paper, we focus on the tunable effects of the lateral equibiaxial tension and the longitudinal prestress on the two-way filtering of FG hyperelastic PCs. The finite structure in our previous work [22] has been proved to be long enough, for which the transmission spectrum as a whole agrees quite well with the band structure of the infinite periodic structure. Therefore, the finite structure considered in this study also consists of 12 A layers and 11 B layers and the undeformed total thickness is $D = 12h_A + 11h_B$.

We have also simulated wave propagations in PCs made of 11 A layers and 11 B layers in both cases of homogeneous and FG material properties. The numerical results indicate that there are two resonant peaks in the first band gap for waves propagating from left to right, but there is no resonant peak for the opposite waves. Thus, we cannot realize the two-way unidirectional wave transmission as in PCs made of 12 A layers and 11 B layers [22].

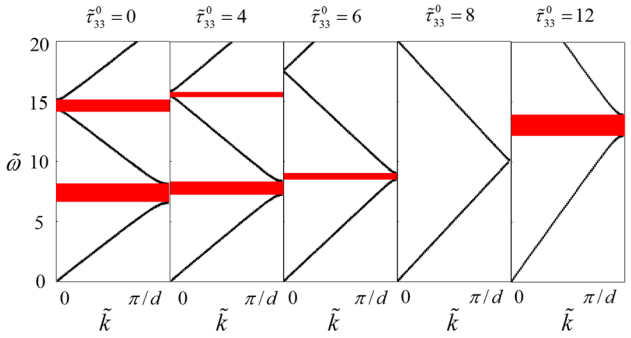

Fig. 2 Dispersion relations of the nongraded PC of Gent model under different prestresses

Nevertheless, it is of great interest to know the effects of structural topology on the wave propagation in finite PCs, which will be studied in a further study.

3.1 Influence of Predeformation on Dispersion Behavior. We first study the band structures of the nongraded PCs. Figure 2 gives the dispersion curves of the PC with a fixed lateral equibiaxial prestretch $\lambda_1 = 1$ but subject to different prestresses. It can be observed that due to the strain-stiffening effect, the first two band gaps have a trend to move upward as $\tilde{\tau}^0_{33}$ increases. Here, $\tilde{\tau}^0_{33}$ denotes the normalized longitudinal prestress along the x_3 direction.

It is interesting to see that band gaps close and reopen in the vicinity of $\tilde{\tau}^0_{33} = 8$. When band gaps close, the elastic waves are able to pass through the structure at any frequency. In order to explain this phenomenon, we need to introduce the acoustic impedance defined by $\sqrt{\rho_p A_{03333p}}$, which equals the product of wave velocity and mass density and is a well-known parameter which characterizes the wave propagation in a solid. Figures 3(*a*) and 3(*b*) plot the acoustic impedance and λ_{3p} as functions of $\tilde{\tau}^0_{33}$, respectively. One could draw a conclusion that as the prestress increases, the acoustic impedance of material B, although smaller when $\tilde{\tau}^0_{33} = 0$, grows more rapidly than that of material A. When $\tilde{\tau}^0_{33}$ is around 8, the acoustic impedances of the two phases intersect, and as a result the band gap vanishes. The underlying mechanism is easy to understand: Since material B is softer, the deformation of layer B under the prestress is larger, and thus material B reaches the strain-stiffening stage earlier. As a result, the effective material properties and volume fraction of layer B become larger than those of layer A after a critical value of the prestress. Besides, from Fig. 3(*b*) we see that the slope of the λ_{3p}–$\tilde{\tau}^0_{33}$ curve decreases as $\tilde{\tau}^0_{33}$ increases, illustrating the strain-stiffening effect clearly.

To study the tunable effect of the prestress on hyperelastic PCs of neo-Hookean model, we take $J_m = 1000$. Figure 4 shows the dispersion curves of the nongraded PC of neo-Hookean model under different values of $\tilde{\tau}^0_{33}$. In contrast to the Gent model, the

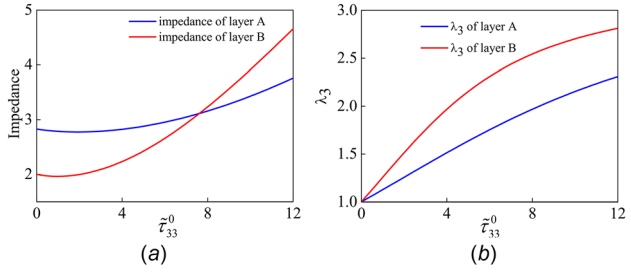

Fig. 3 Variations of (*a*) acoustic impedance and (*b*) stretch along the x_3 direction with prestress for the nongraded PC of Gent model

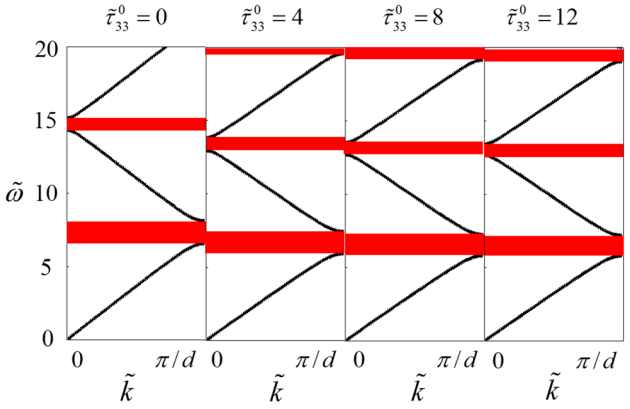

Fig. 4 Dispersion relations of the nongraded PC of neo-Hookean model under different prestresses

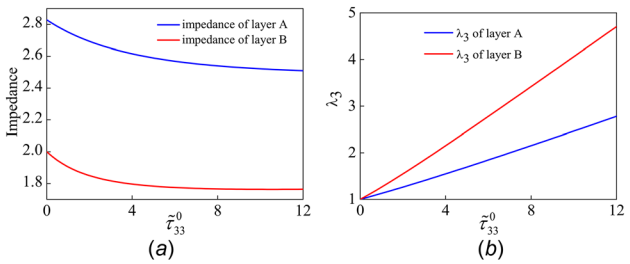

Fig. 5 Variations of (*a*) acoustic impedance and (*b*) stretch along the x_3 direction with prestress for the nongraded PC of neo-Hookean model

band gap frequency for the neo-Hookean model decreases slightly with the increase of the prestress, which is obviously due to the absence of the strain-stiffening effect.

Similar to Fig. 3, the variations of the acoustic impedance and λ_{3p} with the prestress are depicted in Fig. 5 for the neo-Hookean model. Note that with the increase of $\tilde{\tau}^0_{33}$, both the acoustic impedances of materials A and B decrease slightly and tend to be constants. This explains why the band gaps of PCs are lowered down a little for the neo-Hookean model. In addition, λ_{3p} almost depends linearly on $\tilde{\tau}^0_{33}$. Because the impact of the change in prestress on the material of the neo-Hookean model is not very obvious as shown by this example, we will pay attention only to the compressible Gent model with strain-stiffening effect in the following numerical calculations.

Different from Fig. 2, we now investigate the tunable band gaps via changing the equibiaxial tension from 0.8 to 1.4 with the prestress fixed as $\tilde{\tau}^0_{33} = 4$. The results are presented in Fig. 6. It is seen that the band gaps rise with the increase of λ_1, and the band gaps do not vanish but get widened. Figures 7(*a*) and 7(*b*) illustrate the variations of the acoustic impedances and λ_{3p} with λ_1. We observe that the acoustic impedance ratio of material A over that of material B becomes larger when the equibiaxial tension increases, despite the fact that the acoustic impedances of the two phases are both reduced, and the band gaps lift up due to the increase in stiffness. What's more, it is clearly shown in Fig. 7(*b*) that the length of the unit cell becomes smaller due to the Poisson effect when λ_1 increases.

3.2 Influence of Predeformation on Transmission Characteristics of Finite Functionally Graded Phononic Crystals. After analyzing the band gaps of nongraded PCs, we now make use of FGM in the design as in Ref. [22] to see its effect. We suppose that the shear modulus of the p-phase varies in the form of $\bar{\mu}_p(x_3) = K_p(x_3 - D/2) + \tilde{\mu}_p$ in the undeformed configuration, where K_p denotes the grading degree of material p. As

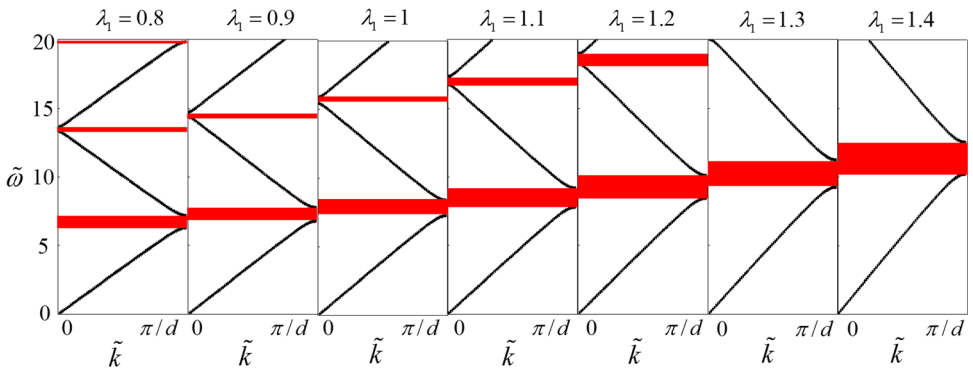

Fig. 6 Dispersion relations of the nongraded PC of Gent model under different equibiaxial tensions and fixed prestress ($\tilde{\tau}_{33}0 = 4$)

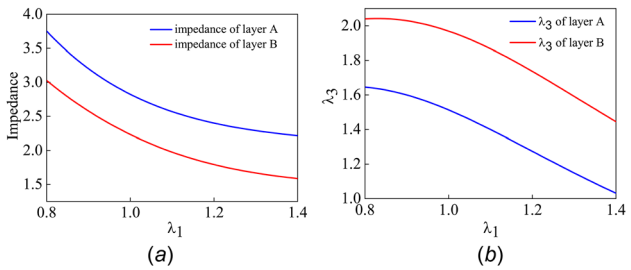

Fig. 7 Variations of (*a*) acoustic impedance and (*b*) stretch along the x_3 direction with equibiaxial tension for the nongraded PC of Gent model

we know, the introduction of spatially varying shear modulus destroys the spatial symmetry of the finite PC and may result in the separation of resonant frequency peaks within the band gap [22]. Our calculation shows that the results by dividing each unit cell into 20 and 22 sublayers are extremely close that the errors can be ignored. Hence, the approximate scheme is considered to be with a good convergence when each unit cell is divided into 20 layers.

The influence of the FG material properties on the band gaps of PCs has been well studied in our previous work [22], which indicates that we can change the separation distances of the two resonant frequency peaks in the band gap by adopting different grading degrees of the FGM for waves propagating in either direction. Just as done for the infinite nongraded PCs, we here first fix $\lambda_1 = 1$ and examine the effect of prestress on the transmission spectrum of the finite FG PC. To display the influences of material grading degrees on wave propagation under mechanical biasing fields, we take $K_A = 0.02$ and $K_B = 0.02$ to enhance the asymmetry of the finite structure. It is noted that the first band gap usually is the commonly used one in engineering applications. Hence, we show the transmission spectra in Fig. 8 around the first band gap

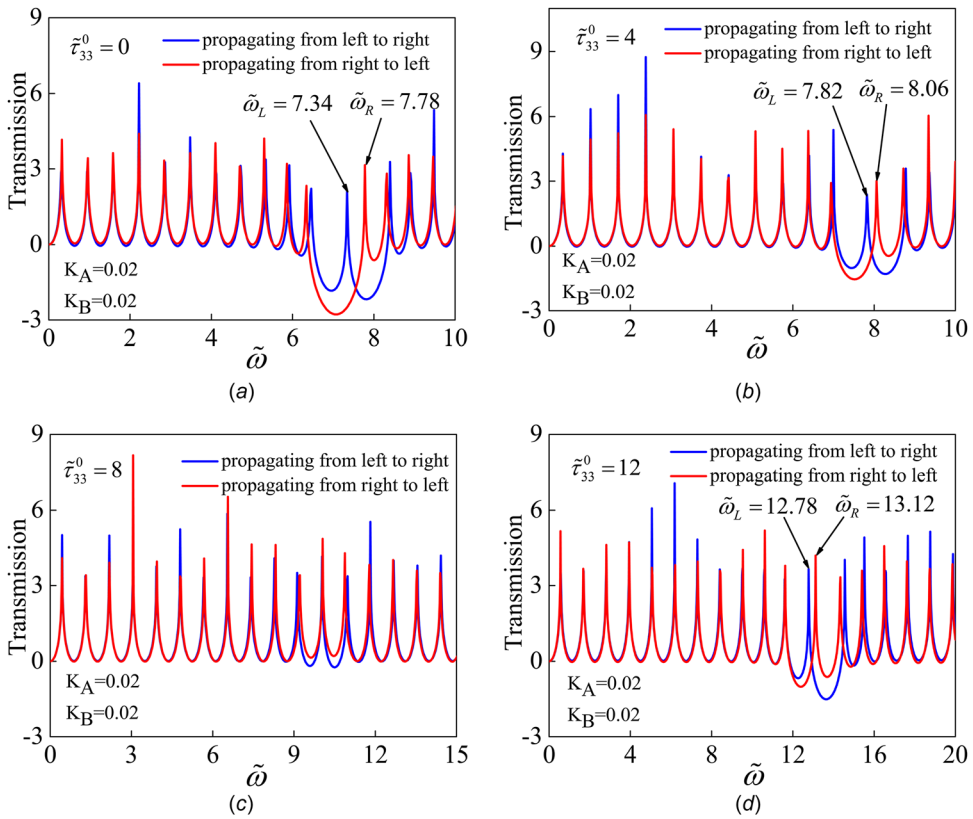

Fig. 8 Transmission spectra under different prestresses ($K_A = 0.02$, $K_B = 0.02$)

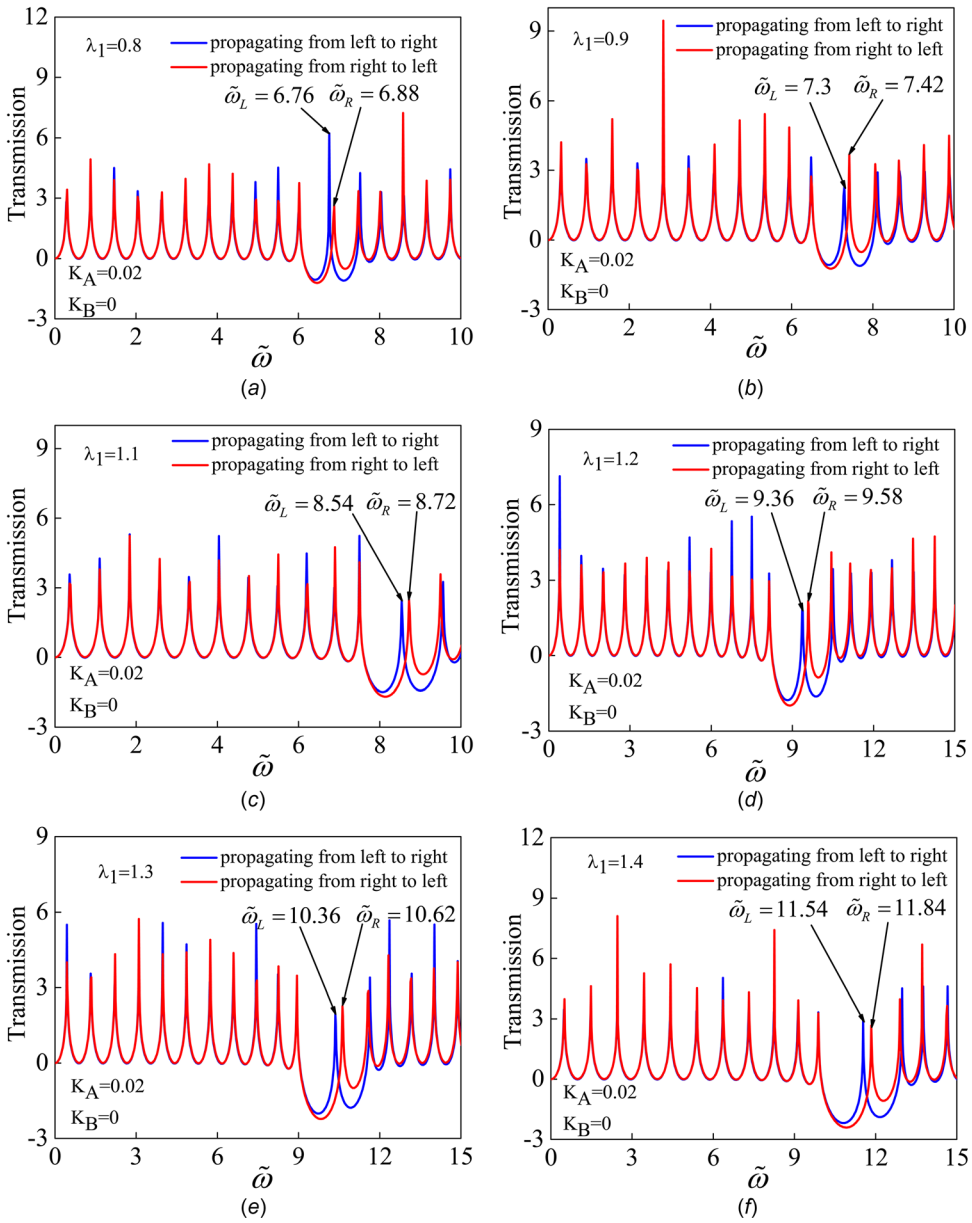

Fig. 9 Transmission spectra at different equibiaxial tensions ($K_A = 0.02$, $K_B = 0$)

under the prestresses $\tilde{\tau}_{33}^0$=0, 4, 8, and 12, respectively. $\tilde{\omega}_L$ and $\tilde{\omega}_R$ indicated in the figure denote the resonant frequencies of waves propagating along opposite directions. It is found from Fig. 8 that when the prestress equals 8 the band gap of the PC will be closed. Also, the resonant frequency peaks outside the band gap are seldom affected by the grading degree of the material. However, we can see from Figs. 8(*a*), 8(*b*), and 8(*d*) that the grading of material properties induces the separation of the resonant frequency peaks in the band gap and asymmetric transmission behaviors in opposite propagation directions are gained. Additionally, $\tilde{\omega}_L$ and $\tilde{\omega}_R$ vary along with the band gap when the prestress changes. Thus, we can conclude that the two-way filtering of the finite FG PC can be effectively tuned by altering the prestress.

We then analyze the influence of the lateral equibiaxial tension on the finite FG PCs by keeping $\tilde{\tau}_{33}^0 = 4$. Without the loss of generality, here material A is regarded as FG and material B is kept homogeneous (i.e., by assuming $K_A = 0.02$ and $K_B = 0$). Figure 9 displays the two-way transmission spectra of the finite FG PC corresponding to different values of λ_1 under the constant prestress. The transmission spectra are consistent with the band structures of the nongraded PC as given in Fig. 6, where the frequency of the first band gap grows up with the equibiaxial tension. The resonant frequencies in the band gap depend on the position of the band gap, which is similar to the results caused by changing the prestress. By altering the value of λ_1, we can also fulfill the tunable asymmetric two-way filtering of waves in the band gap. Besides, we can see that the frequency difference between the resonant peaks $\tilde{\omega}_R - \tilde{\omega}_L$ increases with λ_1.

In order to explain the mechanism of two-way filtering clearly, we present the displacement distributions for two oppositely propagating waves at the resonant frequency peaks based on the results in Fig. 9(*f*). Figures 10(*a*) and 10(*d*) show that the wave is able to pass through the structure at the corresponding resonant frequency despite that it decays from the incident side due to the Bragg scattering, and the result agrees well with the so-called surface-localized mode as discussed in Ref. [39]. Moreover, as shown in Figs. 10(*b*) and 10(*c*), waves are blocked to pass through the structure when their frequencies deviate from the resonant peaks.

3.3 Impact of Poisson's Ratio on Tunability of Soft Phononic Crystals. Different from the earlier results about the effects of mechanical biasing fields and grading degrees of

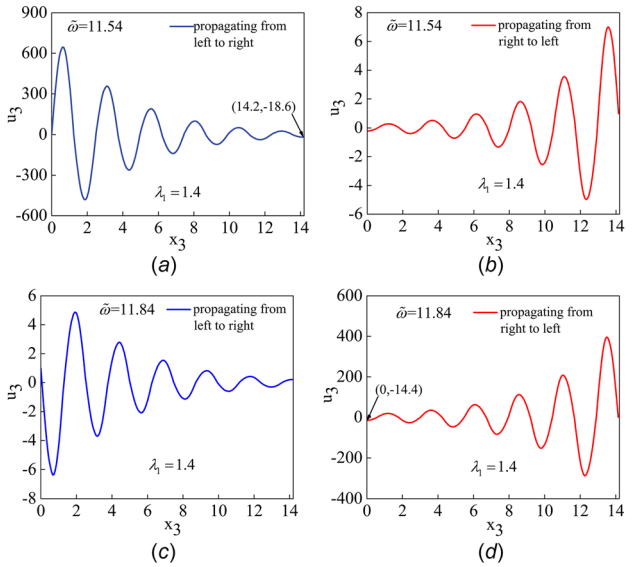

Fig. 10 Displacement distributions of two oppositely propagating waves at the respective resonant frequency peaks ($\tilde{\omega} = 11.54, 11.84$)

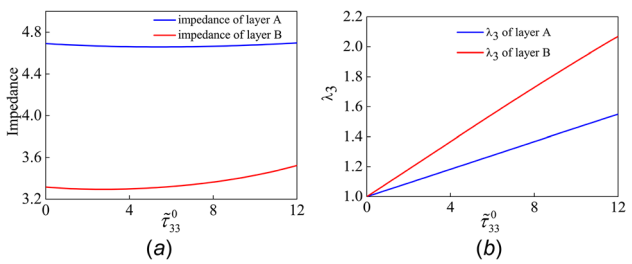

Fig. 11 Variations of (*a*) acoustic impedance and (*b*) stretch along the x_3 direction with prestress for the nongraded PC of Gent model when $\upsilon_A = \upsilon_B = 0.45$

materials A and B, we also want to study the impact of Poisson's ratio on the tunability of the nongraded PC. For brevity, only variations of the acoustic impedance and λ_{3p} with different mechanical loadings are presented here.

Figure 11(*a*) shows that the acoustic impedances hardly depend on $\tilde{\tau}^0_{33}$, when the prestress increases from 0 to 12. The variation of λ_{3p} given in Fig. 11(*b*) shows the similar results to those of the neo-Hookean model as given in Fig. 5(*b*) when the prestress is in the range from 0 to 12. This is because material B has not reached the strain-stiffening stage when the prestress varies in such a range. Thus, for the material with a larger Poisson's ratio, it needs a larger mechanical load to achieve a pronounced effect on the wave propagation behavior. Similarly, we depict in Fig. 12 the acoustic impedance, λ_{3p}, and the acoustic impedance ratio (impedance of material A over that of material B) at different Poisson's ratios (1/3 and 0.45) as functions of the lateral equibiaxial tension. As we can see in Fig. 12(*a*), the acoustic impedance decreases and the relative change is smaller as compared with the results presented in Fig. 7(*a*) due to the different Poisson's ratios. Figure 12(*b*) shows that λ_{3p} decreases when the equibiaxial tension increases and the layer even shrinks in the x_3 direction when λ_1 reaches a sufficiently large value. Under this circumstance, the curve of the acoustic impedance ratio for $\upsilon_A = \upsilon_B = 0.45$ tends to be flat as shown in Fig. 12(*c*), and it implies that λ_1 does not affect the band structure in an obvious manner. While the relative acoustic impedance for $\upsilon_A = \upsilon_B = 1/3$ increases sharply as the material with a smaller Poisson's ratio reaches the strain-stiffening stage earlier in the same range of λ_1.

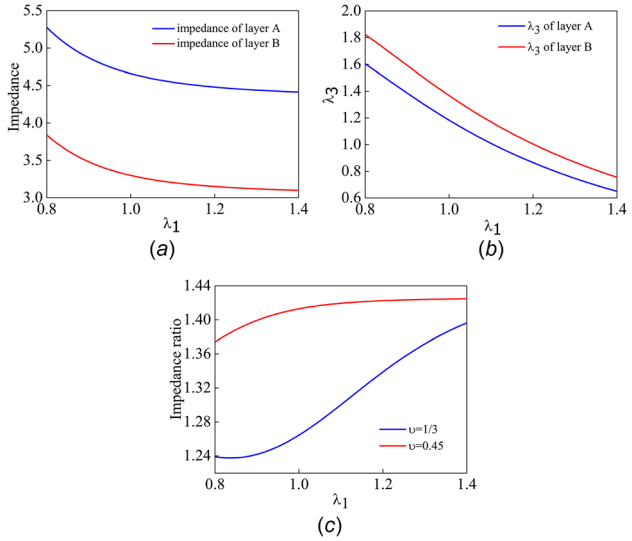

Fig. 12 Variations of (*a*) acoustic impedance and (*b*) stretch along the x_3 direction for $\upsilon_A = \upsilon_B = 0.45$, and (*c*) acoustic impedance ratios for different Poisson's ratios with equibiaxial tension for the nongraded PC of Gent model

4 Summary

This paper illustrated a two-way unidirectional soft acoustic diode that can be tuned by mechanical biasing fields, for the purpose of broadening the operating frequencies. First of all, we described the basic formulations considering the incremental longitudinal wave motions superimposed on the finite deformation caused by mechanical biasing fields. Using the state-space method and approximate laminate technique, we investigated the influences of longitudinal prestress and the lateral equibiaxial tension on the band gaps of nongraded PCs especially for the Gent hyperelastic model, and the transmission characteristics of finite FG PCs, respectively. Through the numerical simulations, we arrived at the following important findings: (1) due to the strain-stiffening effect, the impacts of both prestress and equibiaxial tension on the PCs of the Gent model are more pronounced than the neo-Hookean model. (2) In the vicinity of a certain prestress, the band gap may vanish and reopen with the increase of the prestress, which is very interesting either theoretically or practically. (Nonetheless, this phenomenon does not happen when changing the equibiaxial tension under a constant prestress.) (3) The resonant frequency peaks of waves propagating in opposite directions in the band gap are separated by grading the material property, and the two-way narrow pass-band changes along with the band gap when the PC is subject to external mechanical biasing fields. (4) Poisson's ratio plays a key role in tuning the waves, and in fact the material with a stronger compressibility can be more easily tuned using the mechanical biasing fields. (5) The introduction of acoustic impedance can do us a favor to predict the tunable effect of the mechanical biasing fields.

Making use of the previously mentioned observations and the underlying mechanisms as revealed in the paper, we can design a one-dimensional, effectively tunable two-way acoustic diode. In the band gaps, waves can propagate unidirectionally at the resonant frequency peaks and the operating frequencies can be adjusted easily by changing the mechanical biasing fields. For example, the high-pass filter and low-pass filter may be realized by using soft FG PCs of the Gent model and of the neo-Hookean model, respectively, due to their different performances after controlling the external fields.

Furthermore, we can make the dimensionless Gent constants or mass densities of the two material phases different in a further investigation. Even more measures to tune the acoustic diode can be obtained if we replace the hyperelastic materials with dielectric

elastomers. In summary, the design of tunable acoustic diodes shall be a very interesting and important topic to address in the near future.

Funding Data

- National Natural Science Foundation of China (Grant Nos. 11532001, 11872329, and 11621062, Funder ID. 10.13039/501100001809).
- Fundamental Research Funds for the Central Universities (No. 2016XZZX001-05).
- The Shenzhen Scientific and Technological Fund for R&D (No. JCYJ20170816172316775)

References

[1] Kushwaha, M. S., Halevi, P., Dobrzynski, L., and Djafarirouhani, B., 1993, "Acoustic Band Structure of Periodic Elastic Composites," Phys. Rev. Lett., **71**(13), pp. 2022–2025.

[2] Liu, Z., Zhang, X. X., Mao, Y. W., Zhu, Z. Z., Yang, Z. Y., Chan, C. T., and Sheng, P., 2000, "Locally Resonant Sonic Materials," Science, **289**(5485), pp. 1734–1736.

[3] Liang, B., Yuan, B., and Cheng, J. C., 2009, "Acoustic Diode: Rectification of Acoustic Energy Flux in One-Dimensional Systems," Phys. Rev. Lett., **103**(10), p. 104301.

[4] Wang, X. P., Wan, L. L., Chen, T. N., Liang, Q. X., and Song, A. L., 2016, "Broadband Acoustic Diode by Using Two Structured Impedance-Matched Acoustic Metasurfaces," Appl. Phys. Lett., **109**(4), p. 044102.

[5] Zheng, L. Y., Wu, Y., Ni, X., Chen, Z. G., Lu, M. H., and Chen, Y. F., 2014, "Acoustic Cloaking by a Near-Zero-Index Phononic Crystal," Appl. Phys. Lett., **104**(16), p. 161904.

[6] Zhao, S. D., Wang, Y. S., and Zhang, C., 2017, "High-Transmission Acoustic Self-Focusing and Directional Cloaking in a Graded Perforated Metal Slab," Sci. Rep., **7**(1), p. 4368.

[7] Cummer, S. A., Popa, B. I., Schurig, D., Smith, D. R., Pendry, J., Rahm, M., and Starr, A., 2008, "Scattering Theory Derivation of a 3D Acoustic Cloaking Shell," Phys. Rev. Lett., **100**(2), p. 024301.

[8] Morvan, B., Tinel, A., Vasseur, J. O., Sainidou, R., Rembert, P., Hladky-Hennion, A.-C., Swinteck, N., and Deymier, N., 2014, "Ultra-Directional Source of Longitudinal Acoustic Waves Based on a Two-Dimensional Solid/Solid Phononic Crystal," J. Appl. Phys., **116**(21), p. 214901.

[9] Chen, Y. F., Meng, F., Sun, G. Y., Li, G. Y., and Huang, X. D., 2017, "Topological Design of Phononic Crystals for Unidirectional Acoustic Transmission," J. Sound Vib., **410**, pp. 103–123.

[10] Miyamoto, Y., Kaysser, W. A., Rabin, B. H., Kawasaki, A., and Ford, R. G., 1999, *Functionally Graded Materials: Design, Processing and Applications*, Kluwer, Dordrecht, The Netherlands.

[11] Pompe, W., Worch, H., Epple, M., Friess, W., Gelinsky, M., Greil, P., Hempel, U., Scharnweber, D., and Schulte, K., 2003, "Functionally Graded Materials for Biomedical Applications," Mater. Sci. Eng. A, **362**(1–2), pp. 40–60.

[12] Loy, C. T., Lam, K. Y., and Reddy, J. N., 1999, "Vibration of Functionally Graded Cylindrical Shells," Int. J. Mech. Sci., **41**(3), pp. 309–324.

[13] Chen, W. Q., Wang, H. M., and Bao, R. H., 2007, "On Calculating Dispersion Curves of Waves in Functionally Graded Elastic Plate," Compos. Struct., **81**(2), pp. 233–242.

[14] Cao, X. S., Shi, J. P., and Jin, F., 2012, "Lamb Wave Propagation in the Functionally Graded Piezoelectric–Piezomagnetic Material Plate," Acta Mech., **223**(5), pp. 1081–1091.

[15] Fomenko, S. I., Golub, M. V., Zhang, C., Bui, T. Q., and Wang, Y. S., 2014, "In-Plane Elastic Wave Propagation and Band-Gaps in Layered Functionally Graded Phononic Crystals," Int. J. Solids Struct., **51**(13), pp. 2491–2503.

[16] Guo, X., Wei, P. J., Lan, M., and Li, L., 2016, "Dispersion Relations of Elastic Waves in One-Dimensional Piezoelectric/Piezomagnetic Phononic Crystal With Functionally Graded Interlayers," Ultrasonics, **70**, pp. 158–171.

[17] Torrent, D., Pennec, Y., and Djafari-Rouhani, B., 2014, "Omnidirectional Refractive Devices for Flexural Waves Based on Graded Phononic Crystals," J. Appl. Phys., **116**(22), p. 224902.

[18] Liang, Y. J., Chen, L. W., Wang, C. C., and Chang, I. L., 2014, "An Acoustic Absorber Implemented by Graded Index Phononic Crystals," J. Appl. Phys., **115**(24), p. 244513.

[19] Liang, B., Zou, X. Y., Yuan, B., and Cheng, J. C., 2010, "Frequency-Dependence of the Acoustic Rectifying Efficiency of an Acoustic Diode Model," Appl. Phys. Lett., **96**(23), p. 233511.

[20] Li, X. F., Ni, X., Feng, L., Lu, M. H., He, C., and Chen, Y. F., 2011, "Tunable Unidirectional Sound Propagation Through a Sonic-Crystal-Based Acoustic Diode," Phys. Rev. Lett., **106**(8), p. 084301.

[21] Li, Z. N., Wang, Y. Z., and Wang, Y. S., 2018, "Nonreciprocal Phenomenon in Nonlinear Elastic Wave Metamaterials With Continuous Properties," Int. J. Solids Struct., **150**, pp. 125–134.

[22] Chen, Y. J., Huang, Y., Lü, C. F., and Chen, W. Q., 2017, "A Two-Way Unidirectional Narrow-Band Acoustic Filter Realized by a Graded Phononic Crystal," ASME J. Appl. Mech., **84**(9), p. 091003.

[23] Goffaux, C., and Vigneron, J. P., 2001, "Theoretical Study of a Tunable Phononic Band Gap System," Phys. Rev. B, **64**(7), p. 075118.

[24] Wang, Y. Z., Li, F. M., Huang, W. H., Jiang, X. A., Wang, Y. S., and Kishimoto, K., 2008, "Wave Band Gaps in Two-Dimensional Piezoelectric/Piezomagnetic Phononic Crystals," Int. J. Solids Struct., **45**(14–15), pp. 4203–4210.

[25] Wang, L. F., and Bertoldi, K., 2012, "Mechanically Tunable Phononic Band Gaps in Three-Dimensional Periodic Elastomeric Structures," Int. J. Solids Struct., **49**(19–20), pp. 2881–2885.

[26] Huang, Y., Chen, W. Q., Wang, Y. S., and Yang, W., 2015, "Multiple Refraction Switches Realized by Stretching Elastomeric Scatterers in Sonic Crystals," AIP Adv., **5**(2), p. 027138.

[27] Zhang, P., and Parnell, W. J., 2017, "Soft Phononic Crystals With Deformation-Independent Band Gaps," Proc. R. Soc. A, **473**(2200), p. 0865.

[28] Ogden, R. W., 2009, "Incremental Elastic Motions Superimposed on a Finite Deformation in the Presence of an Electromagnetic Field," Int. J. Non-Linear Mech., **44**(5), pp. 570–580.

[29] Huang, Y., Shen, X. D., Zhang, C. L., and Chen, W. Q., 2014, "Mechanically Tunable Band Gaps in Compressible Soft Phononic Laminated Composites With Finite Deformation," Phys. Lett. A, **378**(30–31), pp. 2285–2289.

[30] Galich, P. I., Fang, N. X., Boyce, M. C., and Rudykh, S., 2017, "Elastic Wave Propagation in Finitely Deformed Layered Materials," J. Mech. Phys. Solids, **98**, pp. 390–410.

[31] Wu, B., Zhou, W. J., Bao, R. H., and Chen, W. Q., 2018, "Tuning Elastic Waves in Soft Phononic Crystal Cylinders Via Large Deformation and Electromechanical Coupling," ASME J. Appl. Mech., **85**(3), p. 031004.

[32] Wu, B., Su, Y. P., Chen, W. Q., and Zhang, C. Z., 2016, "On Guided Circumferential Waves in Soft Electroactive Tubes Under Radially Inhomogeneous Biasing Fields," J. Mech. Phys. Solids, **99**, pp. 116–145.

[33] Dorfmann, A., and Ogden, R. W., 2010, "Electroelastic Waves in a Finitely Deformed Electroactive Material," IMA J. Appl. Math., **75**(4), pp. 603–636.

[34] Zhu, J., Chen, H. Y., Wu, B., Chen, W. Q., and Balogun, O., 2018, "Tunable Band Gaps and Transmission Behavior of SH Waves With Oblique Incident Angle in Periodic Dielectric Elastomer Laminates," Int. J. Mech. Sci., **146–147**, pp. 81–90.

[35] Bian, Z. G., Peng, W., and Song, J. Z., 2014, "Thermal Tuning of Band Structures in a One-Dimensional Phononic Crystal," ASME J. Appl. Mech., **81**(4), p. 041008.

[36] Wu, B., Su, Y. P., Liu, D. Y., Chen, W. Q., and Zhang, C. Z., 2018, "On Propagation of Axisymmetric Waves in Pressurized Functionally Graded Elastomeric Hollow Cylinders," J. Sound Vib., **421**, pp. 17–47.

[37] Wang, P., Shim, J. M., and Bertoldi, K., 2013, "Effects of Geometric and Material Nonlinearities on Tunable Band Gaps and Low-Frequency Directionality of Phononic Crystals," Phys. Rev. B, **88**(1), p. 014304.

[38] Chen, W. Q., and Ding, H. J., 2002, "On Free Vibration of a Functionally Graded Piezoelectric Rectangular Plate," Acta Mech., **153**(3–4), pp. 207–216.

[39] Mizuno, S., 2001, "Theoretical Study on Resonant Transmission of Acoustic Phonons Propagating Through a Superlattice-Liquid Interface," Phys. Rev. B, **63**(3), p. 035301.